2018

A RECTENNA FOR 5G ENERGY HARVESTING

Panagiotis Efthymakis
efthymakisp

Thesis and Dissertations

Graduate School

2018

A RECTENNA FOR 5G ENERGY HARVESTING

Panagiotis Efthymakis

Virginia Commonwealth University

A RECTENNA FOR 5G ENERGY HARVESTING

A thesis submitted in partial fulfillment of the requirements for the degree of Master of Science at Virginia Commonwealth University.

By

PANAGIOTIS EFTHYMAKIS

BSc Informatics & Telecommunications,
University of Peloponnese, Tripolis, Greece 2014

Advisor: AFRODITI VENNIE FILIPPAS, PH.D.

PROFESSOR ELECTRICAL AND COMPUTER ENGINEERING

Virginia Commonwealth University

Richmond, Virginia

May 2018

Acknowledgment

I would like to recognize my adviser Dr. Afroditi Filippas who supported me throughout my thesis project and helped me understand the various parts of it to make this project possible. Her support and guidance contributed to highlight the essential parts of development in both hardware and software to come up with satisfying results and outcomes.

I would also like to thank Dr. Erdem Topsakal for giving me access to his research lab to use the equipment. Finally, I would like to thank Dr. Ding-Yu Fei who agreed to be member in this committee.

This MSc thesis is dedicated to:

My uncle and my aunt, Diomedes and Fay Logothetis

My family, Stylianos Efthymakis, Andriani Vaina and Kalliopi- Eirini Efthymaki

Table of Contents

Table of figures

List of tables

Abstract

This thesis describes the design of a rectenna that is capable of operating in 5G. 5G's availability will create the opportunity to harvest energy everywhere in the network's coverage. This thesis investigates a Rectenna device with a new proposed topology in order to eliminate coupling between input and output lines and increase the rectification efficiency. Moreover, it is designed to charge a rechargeable battery of 3V, 1mA, with a 4.8mm diameter. The current design describes using one antenna for energy harvesting; this could be expanded to use an antenna array, which would increase the input power. This would lead to higher output currents, leading to the ability to efficiently charge a wide variety of batteries. Because of its small size, the rectenna could be used for the remote charging of an implantable sensor battery or for other applications where miniaturization is a design consideration.

Introduction

The technology of wireless power transfer has existed for many decades now, but only for low frequency power transfer. The future Mobile Network Communication System called 5G (5th Generation), will operate in 2020, introducing a different era in Communication Systems. Currently, the state of the art is 4G, which operates in the frequency range of 2 GHz to 8 GHz [1]. 5G, on the other hand, will operate in the frequency range of 600 MHz to 71 GHz (US) [2]. In addition, due to the increased bandwidth, it will improve the user experience by upgrading the current service in terms of data rate, coverage for users and battery lifetime for devices. This new bandwidth leads to the need to redesign devices that currently operate in 4G. An important device for telecommunications is the rectenna, which provides the ability to wirelessly transfer power to a device or a rechargeable battery. In the first chapter, we present 5G technology and what makes it special. Then we will discuss the wireless power transfer techniques, as well as the rectenna technology. Finally, we discuss in depth all the components that we need to achieve this goal and what we have completed it.

Chapter 1: 5G

5G Network will be able to achieve very high data rates depending on the environment and the number of users. Specifically, for one user in an indoor environment, 5G could offer 1 Gb/s data rate service. In an outdoor environment with a greater number of users, the data rate will decrease, reaching values of up to tens of Mb/s. Furthermore, this high data rate experienced should be achieved in 95% of the covered location [3].

The latency for 5G will depend on the scenario. One case is that of an end-to-end latency, where the total time is from the application layer of the transmitter to the application layer of the receiver. Another case is that of user plane latency, which measures the time to transfer a data packet from the user transmitter to the layer 2/layer 3 of the receiver. The network supports latency of 10ms, but it could reach 1ms for applications needing very low latency [3].

The network capacity will significantly rise since the 5G spectrum will exploit frequencies in the mm-Wave bandwidth. The total estimated new bandwidth for 5G will be 10 GHz [4]. This entire spectrum will provide higher quality of service than that provided by the current 4G network.

A massive number of devices will connect to the network simultaneously. This will support the development of the IoT (Internet of Things), where the use of the network will not have limits on the number of physical users, and will also support devices and machines reaching the number of 1,000,000 devices per km^2 (D2D, M2M) [3] [5].

5G will also be more energy efficient. Energy efficiency is the energy over the whole network defined by the number of bits that can be transmitted per Joule of energy. This

will be achieved through intentional network design and device connectivity, leading to longer battery lifetimes [3]. In 5G, the battery lifetime of the device is going to be increased to up to 3 days for the smartphone [3], and up to ten times longer battery lifetime for lower-power devices [6]. Even for a low-cost machine to machine communication device, up to 15 years of life expectancy are predicted [3]. In regards to sensors and wearable devices in 5G, their battery needs to operate without recharging for several years. Sensors are extremely low cost and consume very low amounts of energy in order to sustain long battery life [5].

5G will have high resilience and high availability in order to achieve the needed service and emergency case scenarios used in emergency communications. Resilience is the capability of the network to recover from failures (remote self-healing). Availability is defined as the percentage of time the service is available for one specific region and service [3]. As an example, an application in the industry may have packet delivery within 1 ms with a probability higher than 99.99 percent [5].

Reliability in a communication network is defined as the number of packages the receiver (sink) receives successfully from the transmitter (source), always at the appropriate time for each service. The network has to be available in order to be considered reliable. The 5G Network will have 99.99% reliability, depending on the case and the service needed [3].

Security is another essential requirement of 5G. It will have to manage sensitive data in a human/machine/device based communication. Therefore, there is a need for increased security to overcome any threat on the system or change in data. Another reason for high need of security is that 5G will offer services in significant quarters

(mHealth, autonomous cars, etc.). Finally, the security procedures need to be over and above the node-to-node and end-to-end current security [3].

Chapter 2: 5G Applications

Besides the cellular mobile communications, 5G will assist in the improvement of applications in daily life. Applications on power grids, hospitals, industry, and transportation will change significantly. Moreover, it will introduce ideas and concepts such as smart-city, smart-car, mhealth, and smart-grid. Proposed applications are discussed in each section below [7].

For a smart power grid, we need to gather the data in a center station with a critical communication system. Applications include intelligent management of power transmission, from the distribution network up to utilization at the end of the grid. Moreover, remote management of the station can increase the efficiency of the whole grid [7].

For communication networks for body area networks, continuous monitoring of patients' vital signs increase the need of a highly reliable and available network, such as 5G. In addition, remote medical treatment can be available in cities that lack physicians. Telemedicine and remote monitoring can be utilized to improve population health. Applications in mHealth include but are not limited to personal health monitoring with wearable devices, telemedicine with remote diagnosis, or even remote surgery. Lastly, tracking of medical equipment can be another application for mHealth [7].

Autonomous cars and transportation could lead to a safer form of public transportation minimizing the number of accidents. The low latency and high data rates of 5G can contribute to autonomous car and traffic systems that safely and efficiently control public transportation. Another application that we can consider is V2V (vehicle-to-vehicle)

communication to avoid collisions, increase the fuel economy and lead to higher levels of safety for the passengers and driver [7].

Smart home and generally smart buildings can assist with energy efficiency and manage the resources for heat, water and electricity. Moreover, continuous monitoring can avoid deterioration of supplies, since the system can track their availability and inform the occupants when they reach a minimum level. [7] [2].

In summary, 5G will offer many benefits. As it was described above, high data rate, mobility, number of users, low latency and of course low energy are the main benefits. One challenge of 5G is the interference between the cells (macro and micro cells to pico cells), since their number is going to be significantly greater. There is also need for a high density of relays and massive MIMO systems in order to overcome the difficulty of penetration for the mm-wave technologies. In addition, because of the high attenuation due to free-space loss, improvement of the energy efficiency is needed and can be solved with the increased number of stations. Finally, hardware implementation tends to be challenging since the size of the components decreases as the frequency increases [8]. Another great challenge is traffic management since 5G will have an enormous amount of users [9].

Chapter 3: Wireless Power Transfer

Wireless Power Transfer (WPT) is the transmission of electrical or magnetic energy without the use of wires. WPT is used in cases where the use of wires for powering a device is either not easy or venturesome [10].

In WPT, we have two main techniques for transmission: the near field coupling and far field coupling. In both cases, there is a transmitter, two “antenna devices”, that can be inductors, capacitors, antennas etc. and a rectifier circuit on the receiver side. Below, we briefly describe the far-field technique, which is the one relevant to this project [10] [11].

In far field techniques, power is transmitted through radio waves. Microwave transmission is more directional, giving the capability of transmitting over longer distances. The frequencies used for microwave WPT are between 300MHz to 300GHz, or wavelengths between 1m to 1mm. The system used for the WPT is called a rectenna (“rectifier” and “antenna”). Rectennas convert the AC signal that is received from a dedicated or an ambient source [12]. It consisted of three main components: the receiving antenna, the rectifier and a matching network/circuit for matching the antenna’s and the rectifier’s impedances, which is used for maximizing the power transfer or minimizing signal reflection from the load. The distance between the transmitter and the receiver can be from a few centimeters to many kilometers, depending on the transmitting power and the application [13] [14]. Antennas are used for microwave transmission [11].

Applications for WPT could be separated in four different categories. First, portable rechargeable electronic devices that are used daily could use WPT. Those devices could be cellphones, laptops, tablets, sensors and any small low power device. Another category where WPT could be used is in biomedical applications where biomedical implants can be charged in real time with a dedicated source powering the implant outside of the body. Electric vehicles are another great category where the main concept is charging the electrical vehicle while it is parked at a power station without the inconvenience and the time-consuming plug-in power cords. Moreover, the idea is not limited to parked vehicles; the vehicle can be wireless powered by chargers on the road while it is moving. Finally, energy harvesting is another great category using WPT, as it is in case of space-based solar power.

Section 3.1: 5G Rectenna

The rectenna consists of five main components (Figure 1). The first component is the antenna, which needs to operate in the operating frequency of interest, in our case $f = 27.5\,GHz$. The next component is the matching network that will match the output impedance of the antenna to the rest of the circuit in order to achieve optimal transmission of the signal from the antenna to the load. The next component is the low pass filter that we use in order to eliminate higher-order harmonics; in our case, we will only need to eliminate the first harmonic, as the diode does not transmit frequencies higher than 80GHz. The next one is the rectifier that consists of a diode that can operate at least in the $K_a band$. Finally, the last part is the DC filter (peak detector) and load that in our case is an RC filter where the resistance is 100 ohm to match the internal resistance of a rechargeable battery [15].

Figure 1: Main components of the rectenna. From left to right: antenna, low pass filter, rectifier diode, and DC filter output.

In our research, we investigate a rectenna topology that decreases the coupling between the input and output microstrip lines in order to achieve rectification with minimal circuit surface area. Our rectenna will operate at 27.5GHz, which is in the 5G frequency range.

Chapter 4: Computational Electromagnetic Software

Computational electromagnetics (CEM) allow us to simulate and model how the electromagnetic fields interact with physical objects and the environment. It is based on the different methodologies for solving systems of partial differential equations. Analysis through these models can give approximate solutions of Maxwell's equations for complex structures, with different media and boundary conditions [16]. These numerical techniques are valuable because they allow the designer to customize and optimize the design, something very difficult, time consuming and expensive if done experimentally [17].

The CEM tools we are using are ANSYS Circuit Designer and ANSYS HFSS (High Frequency Structure Simulator) Designer [18]. ANSYS Circuit Designer models specific microwave, RF, passive and active components and then uses a SPICE-type simulator to perform the final circuit analysis, while HFSS is a Finite Element Method (FEM) solver using Full Wave approach.

Section 4.1: Circuit Designer

Circuit Designer uses a mix of different methods such as Method of Moments (MoM), eigen-mode expansion, and closed-form models to simulate discrete microwave, RF and passive and active components, such as the microstrip line, coupled microstrip lines, bends, but also resistors, capacitors, inductors, diodes, amplifiers, etc. It generates an N-port solution matrix for each component and uses SPICE-like techniques to generate a solution matrix for a circuit comprised of these components. In this way, designers can use the Ansys Circuit Design option to model complex

designs and generate frequency and time-domain behavior for these designs. Circuit Designer also has an “optimize” function that allows users to optimize their design to operate within certain user-defined parameters [16].

Moreover, Circuit Designer provides both time and frequency-domain solutions. In the transient analysis, we can see the output of the voltage, the current and the power at specific points or components of our design. Another analysis we can have is the frequency analysis giving us results of the S, Z and Y parameters of the design, and also the VSWR, providing direct comparison between HFSS and Circuit Designer results.

Section 4.2: HFSS

HFSS stands for High Frequency Structure Simulator and is a commercial CEM software from ANSYS. HFSS is a 3-D solver that uses finite element methods to analyze planar structures. While very powerful and highly accurate, HFSS Design cannot be used to analyze the behavior of our full rectifier circuit, which contains discrete components such as the diode and battery (modeled as a resistor). Thus, a hybrid approach was selected. ANSYS HFSS Designer was used to contrast and compare its results against ANSYS Circuit Designer for identical topologies; then HFSS Circuit Designer was used to complete the design to include the diode and the final capacitive load. The sequence of procedures for verification and design are shown in Figure 2 [19].

Table 1: Comparison of Circuit Designer and HFSS designer

Software	**Circuit Designer**	**HFSS**
Frequency analysis	Yes	Yes
Transient analysis	Yes	No
Lumped component behavior	Yes	No
Distributed component behavior	Yes	Yes
Analysis of complex geometries	Yes, but only if they are available in the library of components	Yes, as long as they are planar

Section 4.3: Plan of action

Taking into account the capabilities of each program – to wit, the accuracy of HFSS vs the versatility of Circuit Designer (which allows for the analysis of the diode behavior as well as provides results in the time domain, allowing us to directly observe the rectification of the input signal), this work presents a design process that capitalizes on the advantages of both programs to demonstrate the viability of our rectifier design.

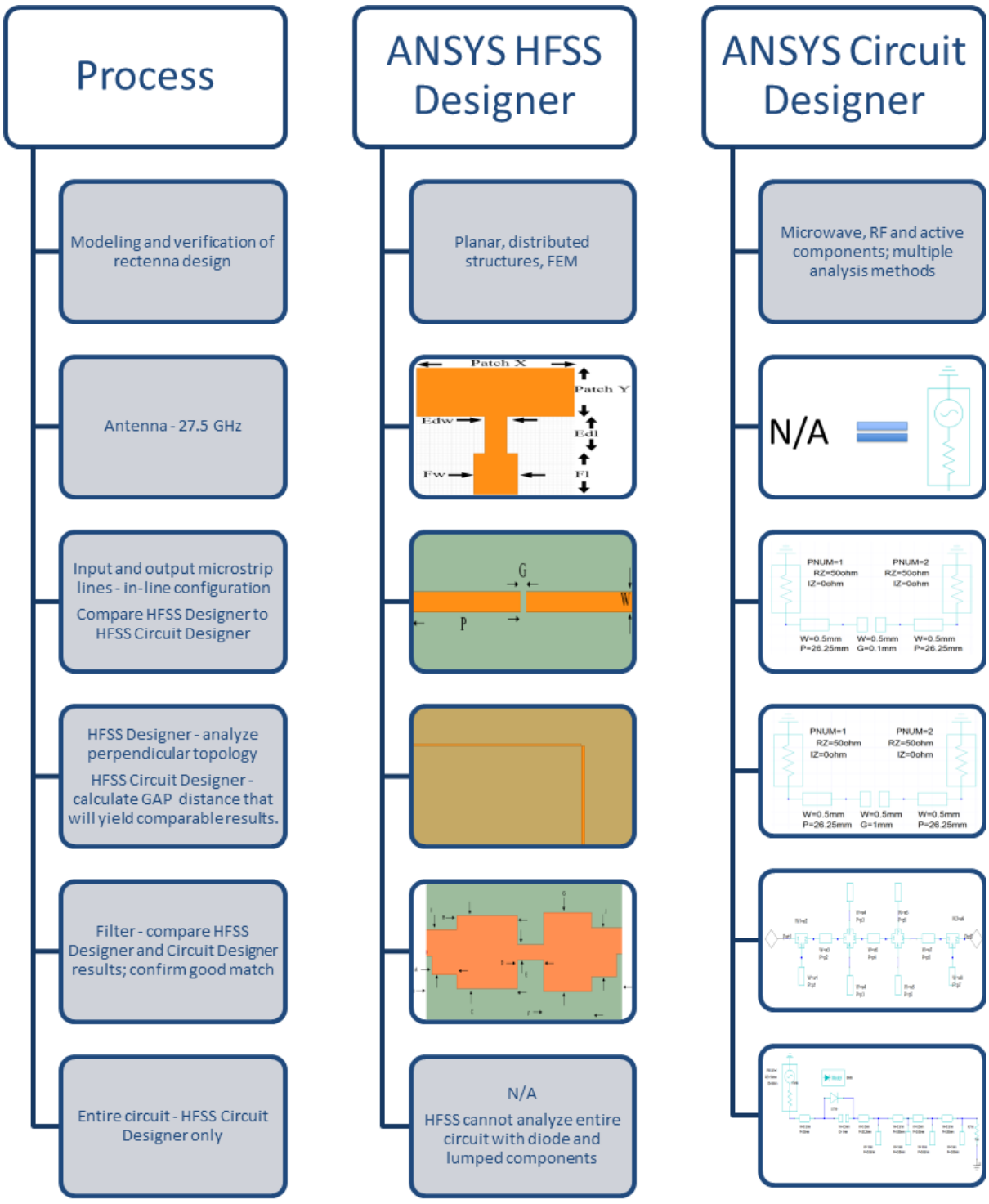

Figure 2: Graph showing the work plan and we utilize each software.

Sequence of events:

1. Antenna design: The patch antenna is initially analyzed using HFSS. In ANSYS Circuit Designer, the antenna is then modeled as an ideal source at 27.5 GHz with an output impedance equal to that calculated through HFSS.

2. Planar topologies: input and output microstrip lines, including modeling gap effects between microstrip lines. Both HFSS and Circuit Designer are used, with results compared in the frequency domain, to confirm good agreement between the two design packages, thus supporting the use of Circuit Designer for the complete circuit.

3. Rectifying circuit with diode, filters and load: Circuit Designer is used to complete the analysis and to demonstrate in the time domain the specific operation of the circuit.

Chapter 5: Antenna

In our project, we designed an edge-fed microstrip patch antenna [20] [21], designed for operation at 27.5GHz with an FR-4 material. The substrate dimensions are $t_{sub} = 0.79mm$ for substrate thickness and $t_{Cu} = 35\mu m$ for thickness of the copper trace. The relative permittivity of the FR-4 material is approximately $\varepsilon_{r(FR-4)} = 4.4$.

Equations (1) and (2) show the width (W) and the length (L) of the patch as a function of the frequency (*f*) and the relative permittivity (ϵ_r) [22].

$$\mathrm{W} = \frac{1}{2\mathrm{f_r}\sqrt{\mu_0\epsilon_0}}\sqrt{\frac{2}{\epsilon_\mathrm{r}+1}} = \frac{\mathrm{u_0}}{2\mathrm{f_r}}\sqrt{\frac{2}{\epsilon_\mathrm{r}+1}} \quad (1)$$

$$\mathrm{L} = \frac{1}{2\mathrm{f_r}\sqrt{\epsilon_\mathrm{reff}}\sqrt{\mu_0\epsilon_0}} - 2\Delta\mathrm{L} \quad (2)$$

Where:

$W = width\ in\ meters\ (m)$

$f_r = operating\ frequency\ in\ Hertz$

$\mu_0 = magnetic\ permeability\ in\ Henries\ per\ meter\ \left(\frac{H}{m}\right)$

$\epsilon_0 = vacuum\ permittivity\ Farad\ per\ meter\ \left(\frac{F}{m}\right)$

$u_0 = speed\ of\ light\ in\ meters\ per\ second\ \left(\frac{m}{s}\right)$

$\epsilon_r = relative\ permittivity$

$\Delta L = edge\ feed\ length\ in\ meters\ (m)$

$\epsilon_{reff} = effective\ dielectric\ constant$

$1 < \epsilon_{reff} < \epsilon_r$

We simulated the antenna design using ANSYS HFSS Designer [18]. After designing the antenna, the dimensions (in Figure 3) for operation at 27.5 GHz are shown in Table 2.

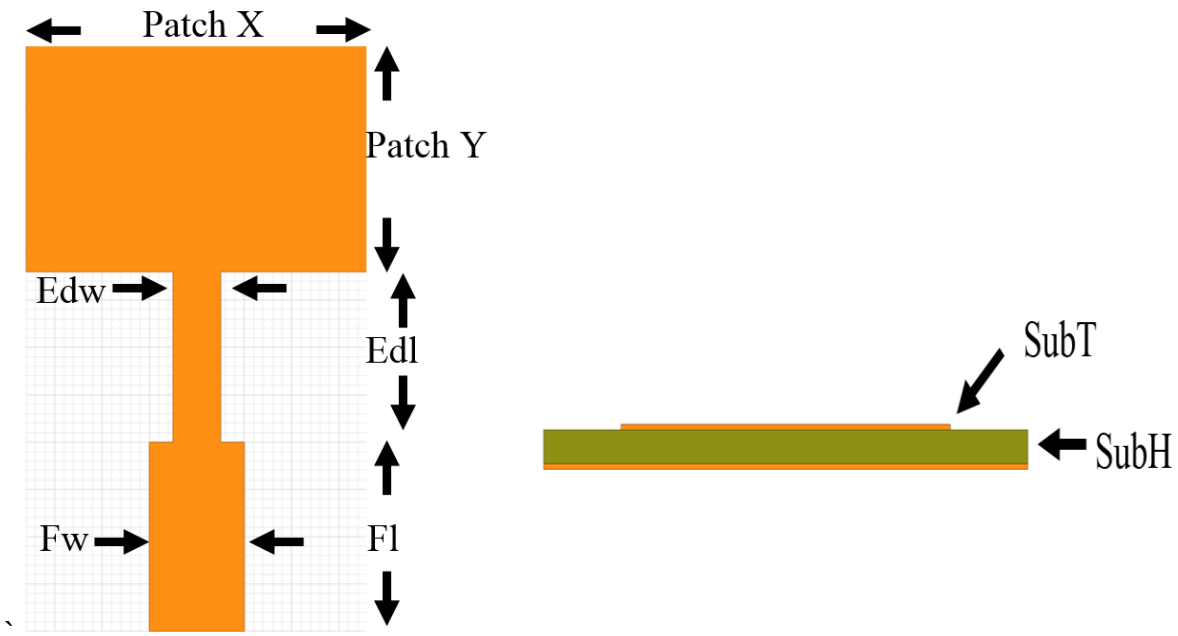

Figure 3: Patch antenna top (left) and side view (right)

We set our simulation from 1 to 50 GHz with step 0.01GHz with 4901 points. The efficiency of the antenna is measured through the return loss, or S_{11}. The antenna will radiate within the frequency range where $S_{11} < -10dB$. The simulation (blue line) results that we had with these dimensions for return loss was $S_{11} = -21.25dB$ (Figure 4) for 27.5GHz. The results for the fabricated antenna are also shown in Figure 4 (red line). As can be seen, the frequency range for which $S_{11} < 10dB$ is $26.52\ GHz < f < 28.58\ \text{GHz}$. The minimum value of S_{11} occurs at $f_{min} = 28.01\ GHz$, which is a 4% error from the desired $f_{min} = 27.5GHz$ (Figure 4).

Table 2: Antenna dimensions and description of each variable.

Variables	Value	Description
Patch X	3.4mm	Patch Width
Patch Y	2.1mm	Patch Length
SubT	35um	Trace thickness
Edw	0.5mm	Edge feed width
Edl	1.9mm	Edge feed length
Fw	1 mm	Feed width
Fl	2 mm	Feed length
SubH	0.72 mm	Substrate Height

In order to fabricate an antenna that will resonate at 27.5 GHz, we first varied the width of the patch (Patch X) from 3.1 mm to 3.6 mm and plotted the resulting resonant frequency (Figure 5). Then, we varied the length of the patch (Patch Y) from 1.9 mm to 2.4 mm and again plotted the resulting resonant frequency (Figure 6). Based on the results of these graphs, we chose a Patch X and Patch Y combination that would theoretically place the resonant frequency at 4.4% away from the desired frequency.

The dependency on frequency for both the width and the length of the patch is linear (Figure 5, Figure 6). Although if we compare the frequency difference for the same change in length, we can easily observe that changing the patch length, Patch Y, more significantly changes the resonant frequency.

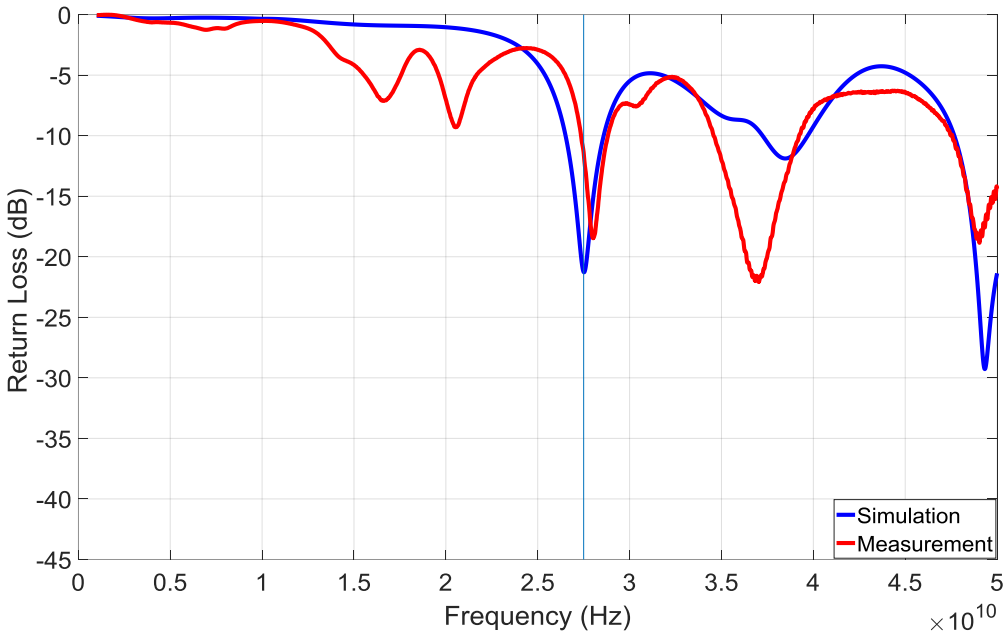

Figure 4: Return loss of the antenna. There is a 4.4% difference from simulation to measurement.

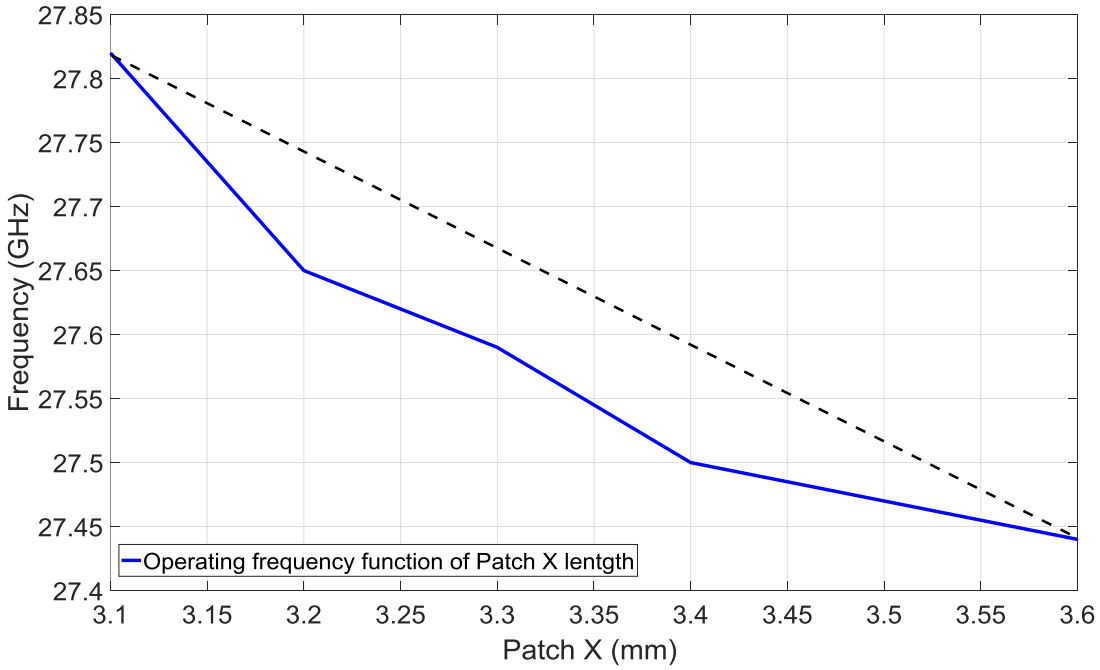

Figure 5: Operating frequency vs. the width of the patch, PATCHX

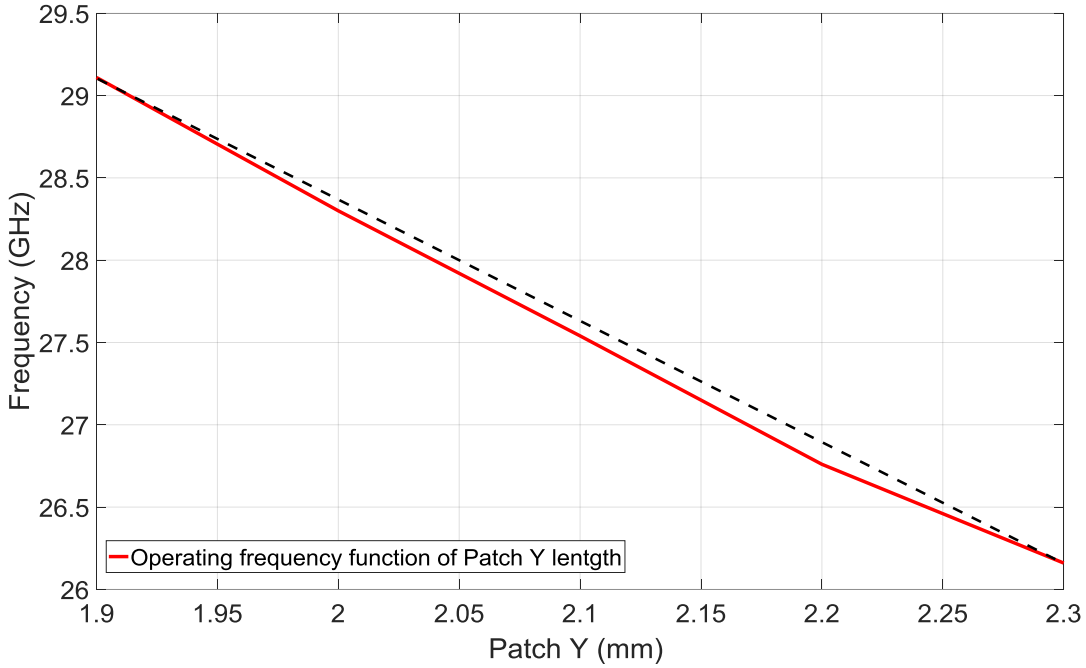

Figure 6: Operating frequency vs. the length of the patch, PATCHY.

Figure 7: Fabricated antenna with the end launch connector

Figure 7 shows the fabricated antenna connected to the end launch connector. The measured results were better with -21.25dB (Figure 8) at 27.5GHz. The simulation (blue line) results that we had with these dimensions for return loss was $S_{11} = -18.5\,dB$ (Figure 8) for $f = 26.1GHz$. For the fabricated antenna, the frequency range for which

$S_{11} < 10dB$ is $26.35\ GHz < f <$ 28.83 GHz . The minimum value of S_{11} occurs at $f_{min} = 27.33GHz$.

In addition, the impedance of the fabrication at 27.5GHz was $Z_{ant} = 43.48 - 3.8$j. Compared to $Z_0 = 50\ ohm$, the real part has a 13% error and the imaginary part has a 7.6% error. A single or a double stub for matching the antenna to the rest of the circuit will be needed.

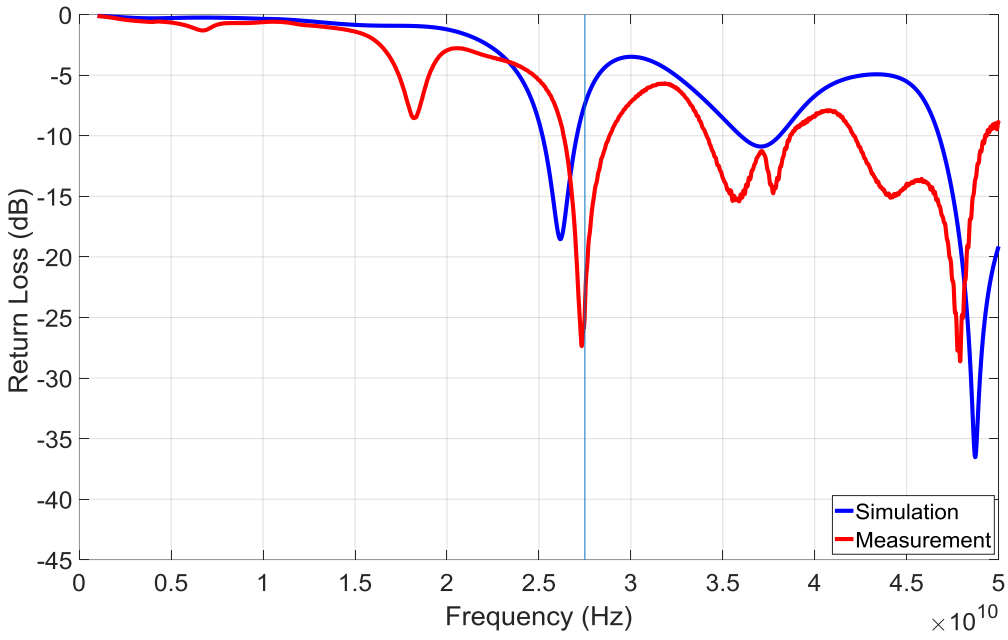

Figure 8: Return loss of the antenna. Change of the Patch Length Y at 2.3mm, giving simulation -18.5GHz at 26.51 and fabrication results -21.25dB at 27.5GHz.

Finally, the Smith chart response showed the impedance of the antenna is $Z_{out,27.5GHz} = 43.48 - j4.8$.

Chapter 6: Low Pass Filter before Diode

We need a low pass filter after the antenna and before the diode to block higher-order harmonics. In our case, for the low pass filter, we need it to block the first harmonic, since the natural operation of the diode blocks anything higher than 80 GHz. Therefore, only the 55 GHz frequency needs to be blocked. The main parameter we need to check for our design is the insertion loss S_{21}. A filter blocks certain frequencies when the insertion loss at those frequencies is below -3dB. Therefore, we need S_{21} to be close to 0dB at 27.5GHz and below -3dB at 55GHz. Our design requirements were a low pass filter with cutoff frequency $f_c = 41.25GHz$ with insertion loss $S_{21} = -15dB$ at 55GHz. For the microwave filter before the diode, we are proposing a fourth order Butterworth filter with microstrip stubs. A Butterworth (also known as maximally flat) filter has a frequency response that it is monotonic in the passband. The higher the order that we use the sharper the filter cutoff will be. The drawback to this is the increased complexity of the design as well as increased losses due to the increased surface area of the metal. We simulated the Butterworth filter for both Circuit Designer (Figure 9) with dimensions on Table 3 and HFSS (Figure 10) with dimensions on Table 4.

Figure 11 shows that Circuit Designer yielded insertion losses of $S_{21} = -0.02\text{dB}$ and $S_{21} = -7.21\text{dB}$ for 27.5GHz and 55GHz respectively. HFSS yielded consistent results, with $S_{21} = -1.23\text{dB}$ and $S_{21} = -5.98\text{dB}$ again for 27.5GHz and 55GHz respectively. Both the values on Circuit Designer and on HFSS are acceptable for a microwave low pass filter.

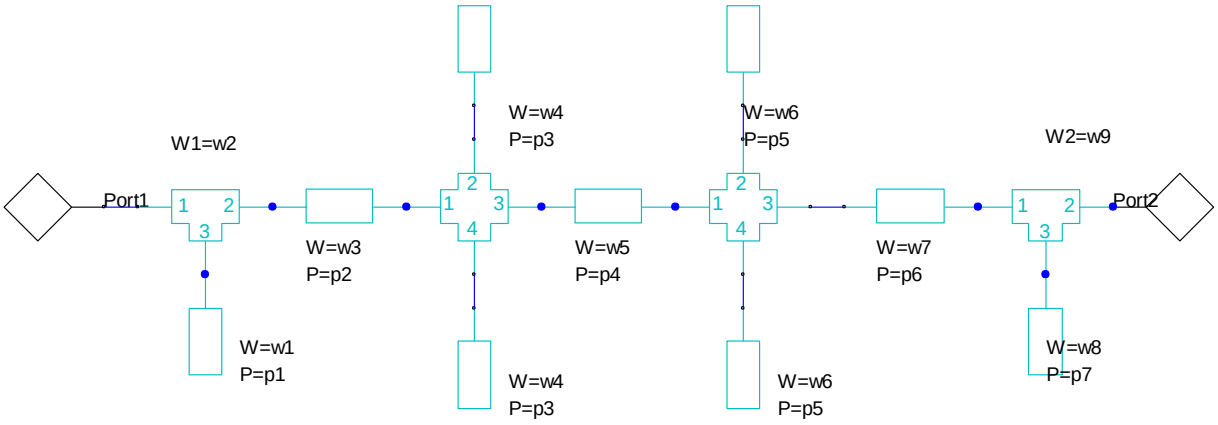

Figure 9: Schematic view of the fourth order Butterworth filter in circuit designer

Table 3: Parameters of the circuit design for the filter dimensions

Name	w1	p1	w2	w3	p2	w4	w5	p3	p4	w6	w7	p5	p6	w8	p7	w9
Value (mm)	0.12	0.38	1.47	0.65	0.51	1.23	0.22	0.2	0.53	0.97	0.7	0.22	0.51	0.14	0.37	1.37

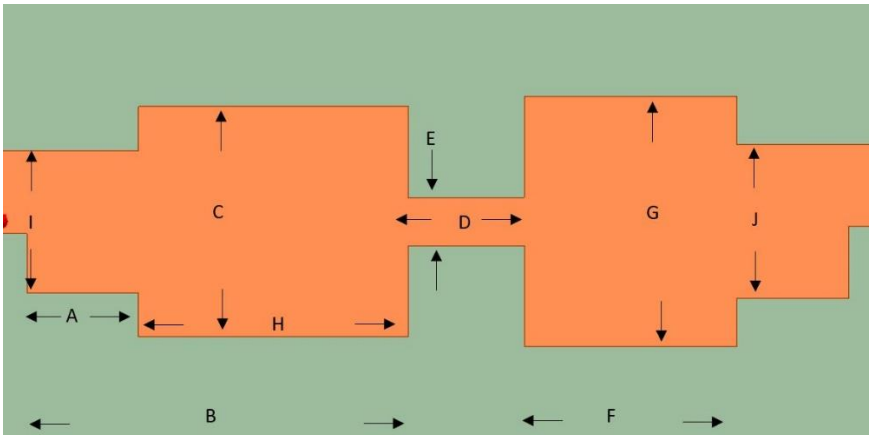

Figure 10: Top view of the fourth order Butterworth filter in HFSS

Table 4: Parameters of HFSS design for the filter dimensions

Length (mm)	0.51	4	1.05	0.53	0.22	0.97	1.14	1.23	0.65	0.7
Name	A	B	C	D	E	F	G	H	I	J

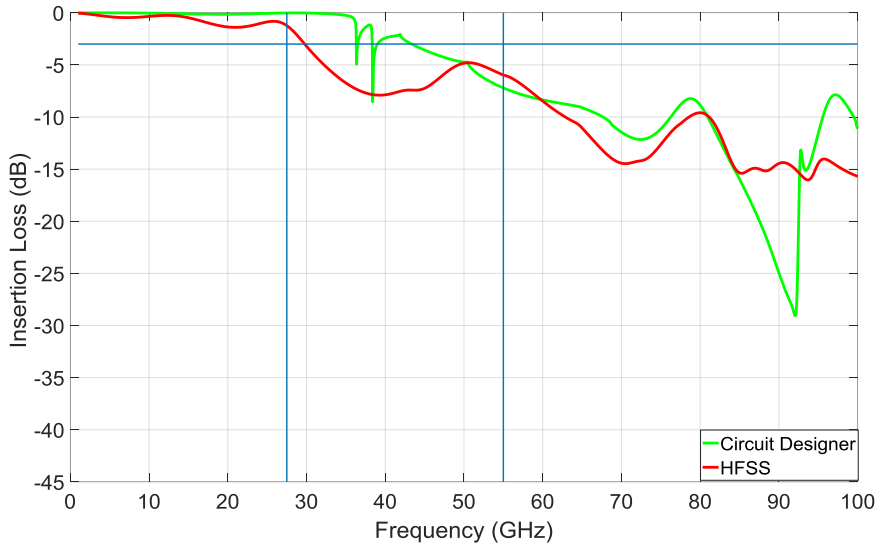

Figure 11: Comparison of circuit designer and HFSS results for the filter response (insertion loss)

Chapter 7: Microstrip lines

At first, we designed a circuit of two microstrip lines with a specific gap. In more detail, in each end we connected a microwave port of $Z_0 = 50\Omega$ impedance. After optimization with Circuit Designer, we chose two microstrip lines, each with width $W = 0.5\,mm$ and length $P = 26.25\,\mathrm{mm}$ (Figure 12). We included the GAP component between the microstrip lines (Figure 13), to simulate the effect of the gap between the two microstrip lines [23]. To be consistent with the length of the diode, we set the gap to be $G = 0.1mm$.

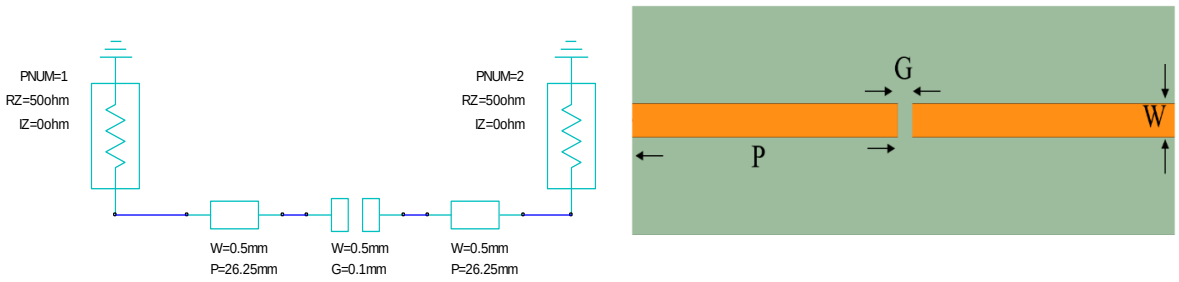

Figure 12: Input and output microstrip lines with gap between the lines. Topology is in-line. (a) ANSYS Circuit Designer simulation. (b) ANSYS HFSS simulation.

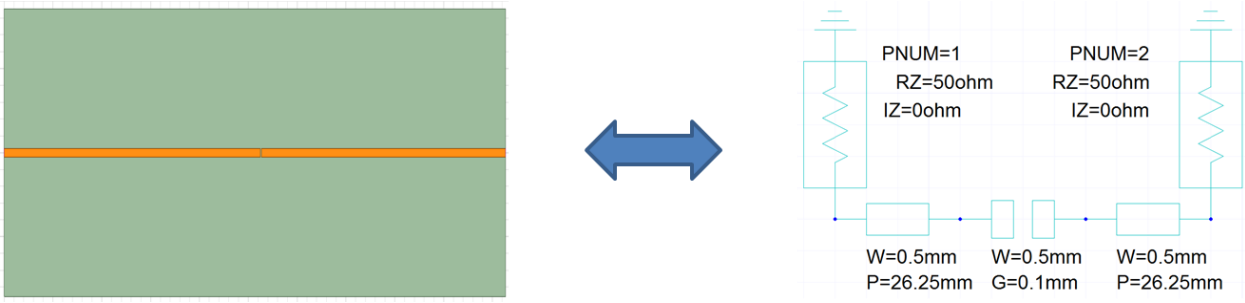

Figure 13: Equivalent circuits from HFSS to circuit design according to insertion loss (inline)

First, we confirmed that the Circuit Designer and the HFSS Designer results agree (Figure 14 and Figure 1) when they simulate the same structure. The structure was two microstrip lines as shown in Figure 13. The first structure analyzed was that of the input and output microstrip lines; the input line takes the signal from the antenna to the diode; the gap isolates the output from the input; this gap will eventually be bridged by the diode, which will perform the rectification of the signal. Without the diode, there should be no signal from the input line to the output line. That is, S_{12} should be at least -10dB. We found, however, that when the input and output lines were placed in the topology in Figure 12 with only a 0.1 mm gap between them, at high frequencies, there was still a signal at the output at the high frequencies which are of interest to us. Thus, we will be proposing to place the input and output lines perpendicular to each other (as in Figure 18). Since this topology does not exist in Circuit Designer, we will present the "equivalent in-line gap" that matches the proposed perpendicular topology. We will use results from HFSS for the perpendicular topology and match them to the corresponding in-line gap from Circuit Designer.

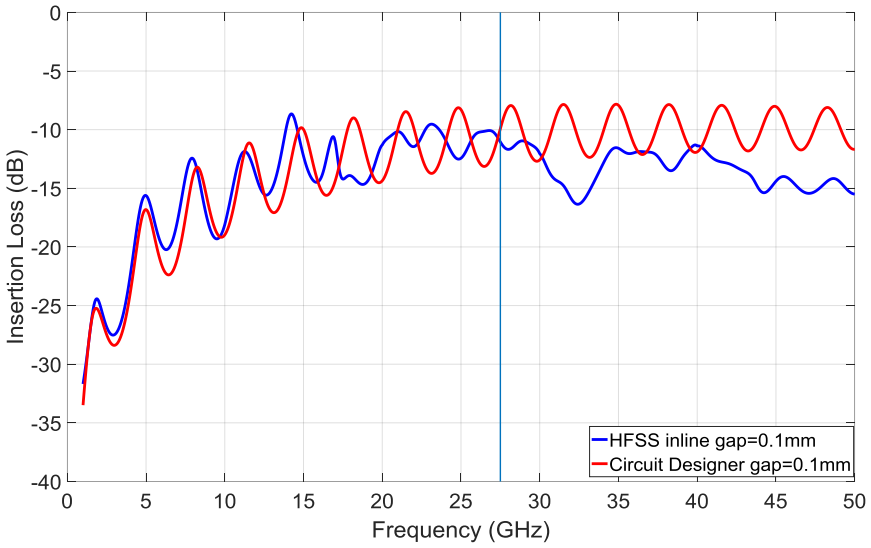

Figure 14: Comparison of Circuit Design and HFSS Design for the same structure of two microstrip lines with gap

Following the literature [24] [25] [26] [27], we will utilize the MA4E1317 MACOM diode. The MA4E1317 is a single gallium arsenide flip chip Schottky barrier diode. The high cutoff frequency of these diodes allows use through V frequency bands. Typical applications include single and double balanced mixers in PCN transceivers and radios, police radar detectors, and automotive radar detectors and rectifier antennas in mmWave frequency bands. The devices can have up to 80 GHz operating frequency.

Parameters of the diode:

$C_j = 0.02\ pF$ Junction Capacitance

$C_t = 0.45pF$ Total capacitance

$R_s = 4\ \Omega$ Series Resistance

$V_{f1} = 0.7\ V$ Forward voltage

$V_{br} = 7\ V$ Reverse Breakdown Voltage

$F_c = 80\ GHz$ Cutoff frequency

By performing a transient analysis on the design in Figure 15, we generate the results shown in Figure 16. The input voltage is $V_g = 900\ mV$, and we chose this because of the output of the current signal generator we had in our lab. Because of the impedance of the port, the input voltage before the diode is $V_{in} = 560mV$. The output is $V_{out} = 166mV$ but instead of having only positive cycles due to the diode, we have negative cycles as well (Figure 16). Those negatives cycles persist because of the coupling that exists at those frequencies, allowing even the negative cycle of the input signal to travel through the gap. In order to decrease the coupling, we need to eliminate the insertion loss S_{21} that is related to the coupling since it shows how much power is transferred to the second port from the first port. We need to have both minimum return loss (S_{11}) and minimum insertion loss (S_{21}). The S_{11} will have to be minimum so there is less reflection to the input signal. We also need to minimize the insertion loss in order to decrease the coupling between the microstrip lines in the essential point where we have the diode.

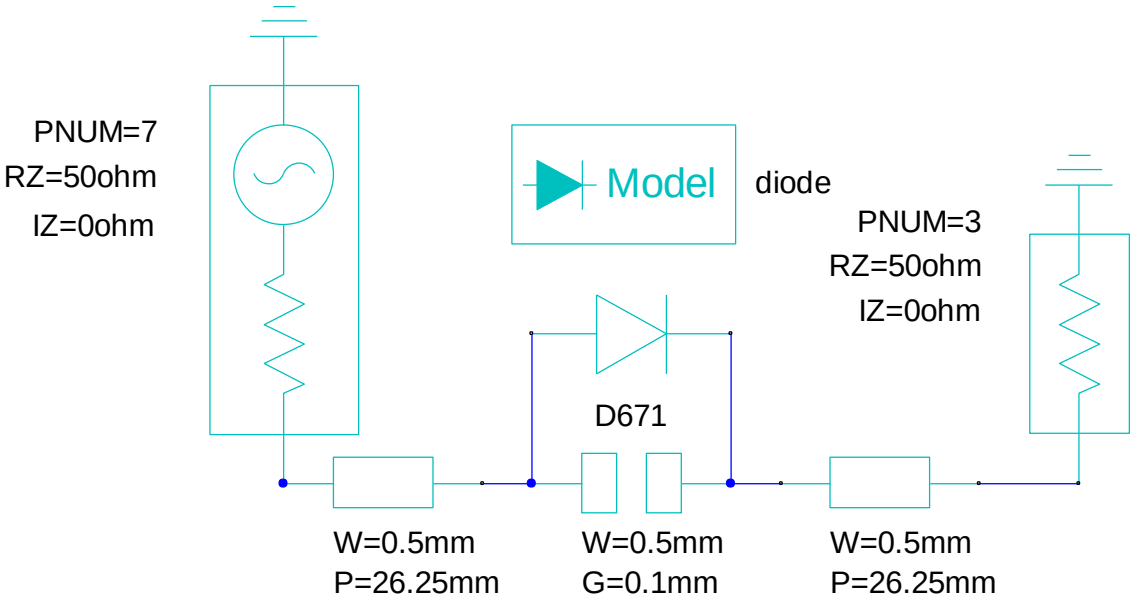

Figure 15: Two microstrip lines connected with a microwave diode

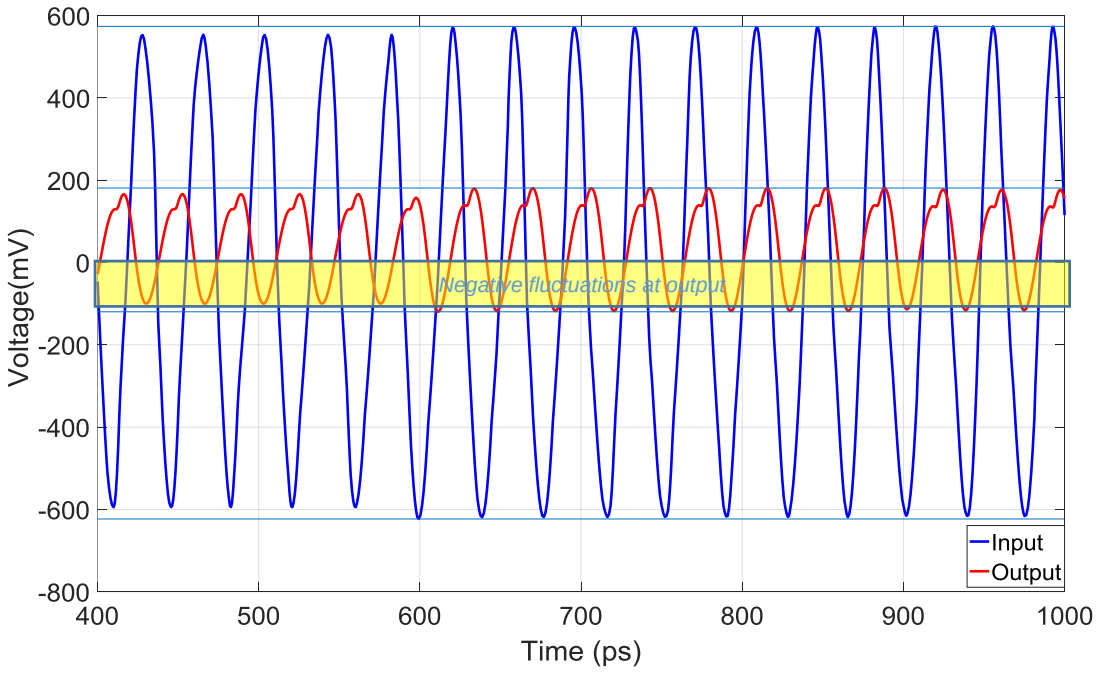

Figure 16: Transient analysis with input 900mV and gap 0.1mm on circuit designer

First, we need to check the return loss and insertion loss to be minimum. So in Figure 17 we can see that $S_{11} = -5\text{dB}$ and $S_{21} = -10\text{dB}$.

Secondly, we changed the topology from in-line to perpendicular using only HFSS (Figure 18). The new topology (Figure 18) has the same separation between the corners of the microstrip lines as the original gap in the in-line topology. We subsequently examined the insertion loss for each topology. Figure 19 shows that the insertion loss of in-line topology was $S_{21} = -11\text{dB}$ while for perpendicular $S_{21} = -24\text{dB}$ at 27.5GHz.

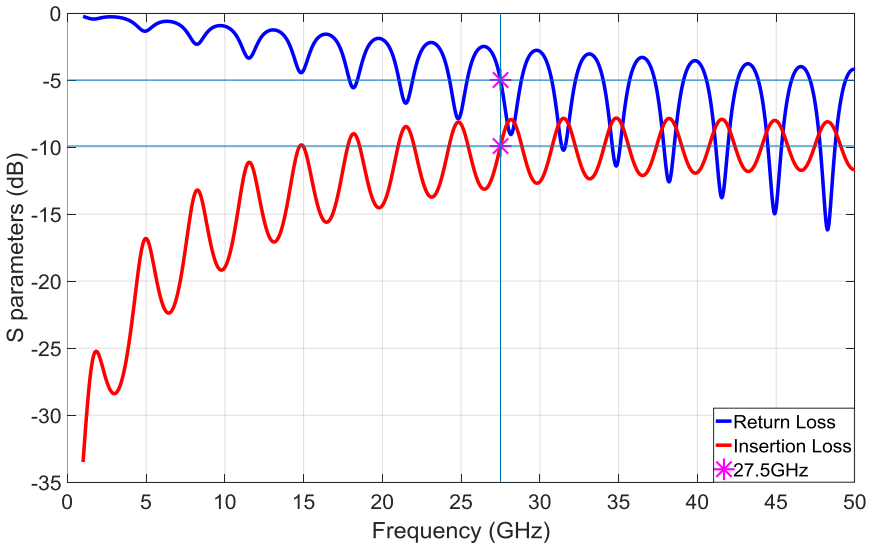

Figure 17: Return and Insertion Loss for two microstrip lines in Circuit Designer

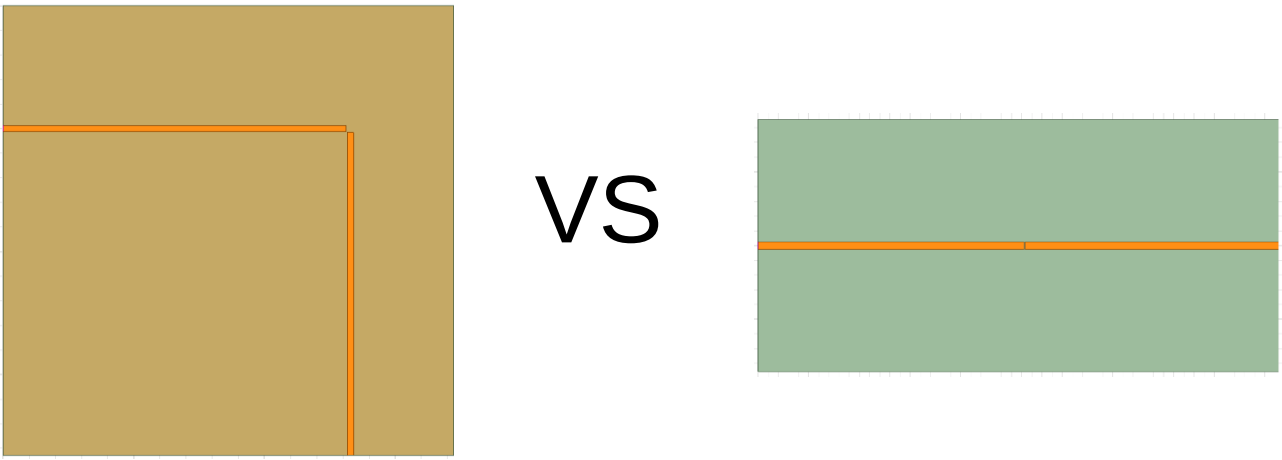

Figure 18: Perpendicular topology in HFSS with gap-0.1mm vs in-line topology with the same gap. In the perpendicular topology, the gap is corner-to-corner, whereas in the perpendicular topology, the gap is across the entire width, allowing for better signal cross

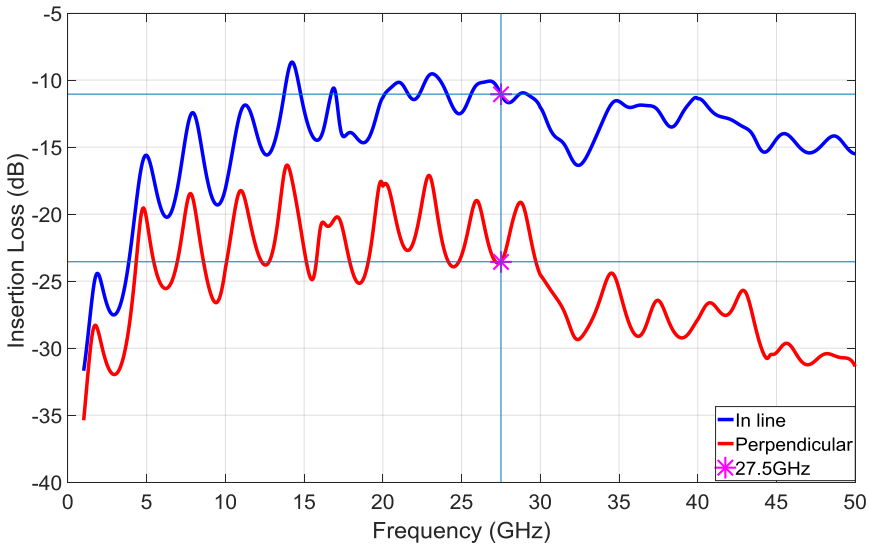

Figure 19: Comparison of insertion loss for the in-line to the perpendicular topology; HFSS. Note that the insertion loss for the perpendicular topology is significantly lower than that of the in-line topology at high frequencies.

The next step was to compare the return loss for these two topologies. Both of them had a $S_{11} = -4dB$ return loss as we can see in Figure 20.

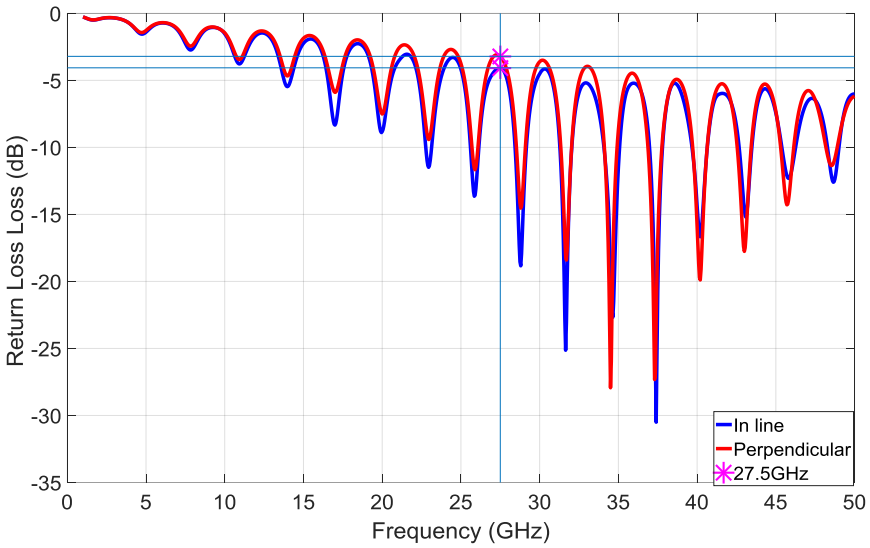

Figure 20: Comparison of in line to perpendicular topology as concerns the return loss (S_{11}) on HFSS

Thus, by comparing the perpendicular topology in HFSS with the in-line and gap topology with Circuit Designer, we found that a 0.1 mm gap in the perpendicular topology (Figure 21) is equivalent to a 1 mm gap in the in-line topology. Since the entire circuit can only be simulated in Circuit Designer, we use the in-line input and output microstrip lines with a 1 mm gap to simulate the perpendicular topology with a 0.1 mm gap (Figure 22)

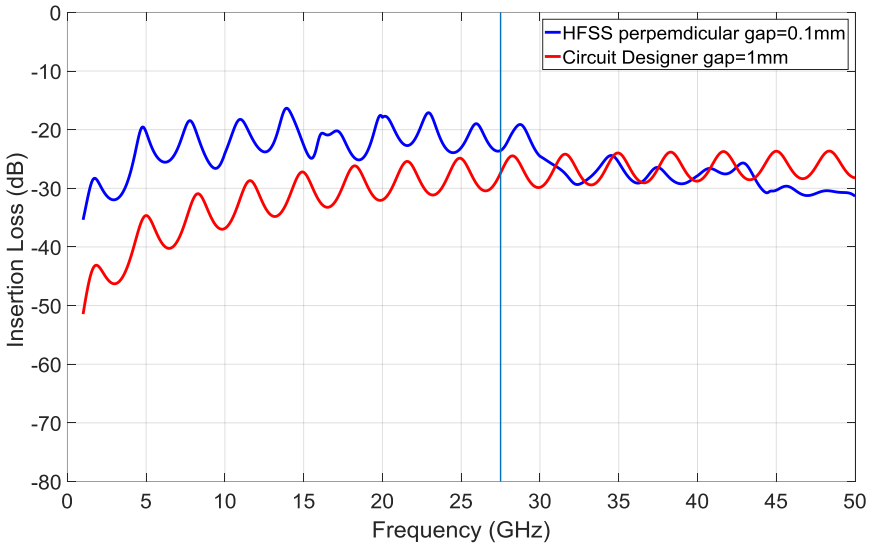

Figure 21: Comparison of insertion loss of perpendicular topology with gap=0.1mm and Circuit Designer Gap topology with gap 1mm

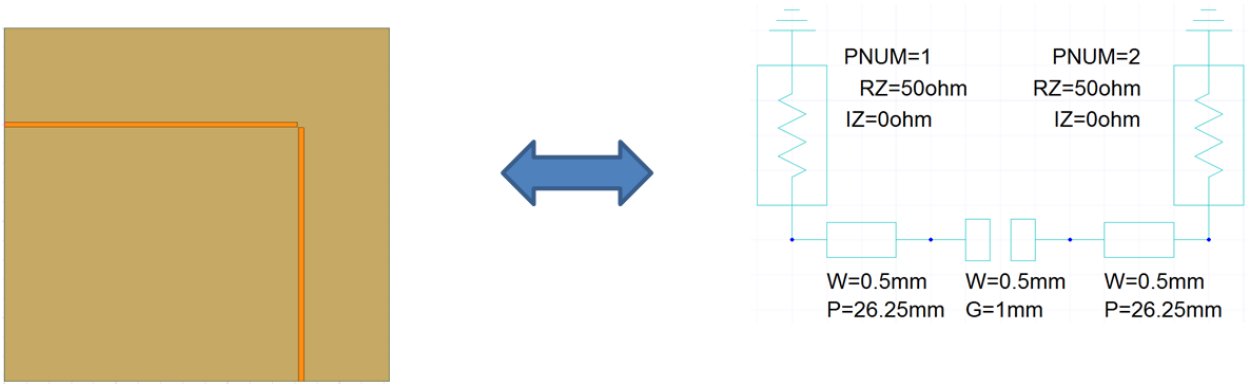

Figure 22: Equivalent circuits from HFSS to circuit design according to insertion loss (perpendicular)

The next step was to fabricate these designs and confirm that this perpendicular topology decreases the coupling. We fabricated the topologies with the use of milling machine, and then tested their response with the network analyzer (Figure 23).

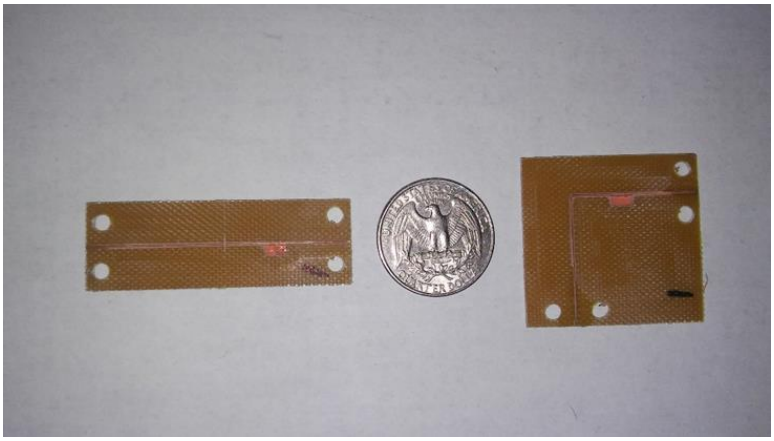

Figure 23: On the left the fabricated in line topology and on the right the fabricated perpendicular one. Both of them they have a rectangular metal trace next to the second line for ground.

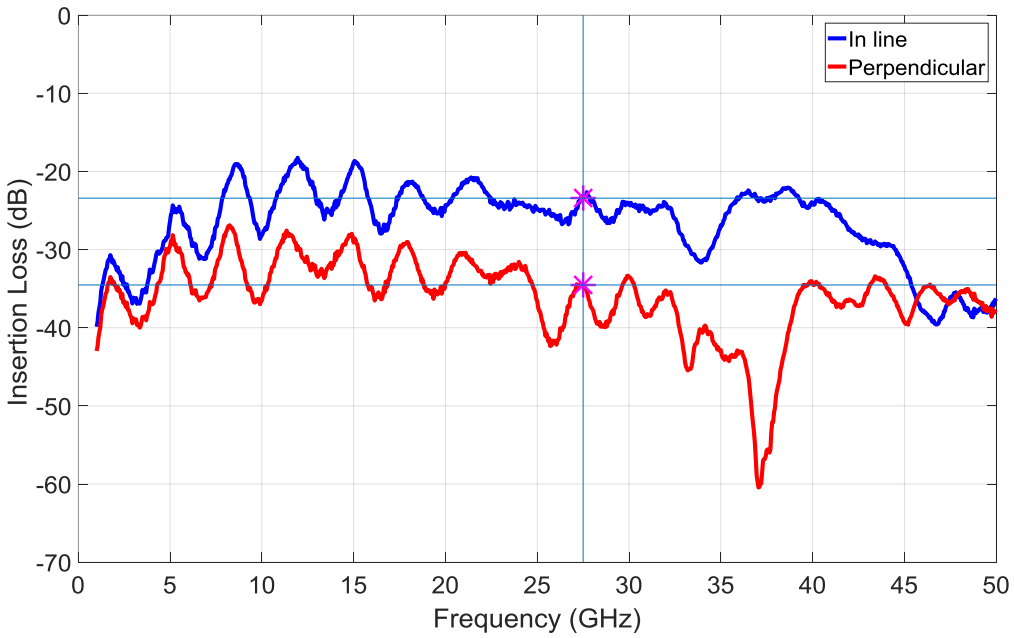

Figure 24: Comparison of in line to perpendicular topology as concerns the insertion loss (S_{21}) for the fabricated designs

The results from the network analyzer confirmed the simulations. As we can see in Figure 24, the in-line topology had $S_{21} = -23\text{dB}$ while the perpendicular topology had $S_{21} = -34\ dB$.

After confirming that the perpendicular topology decreases the coupling (Figure 24) we assumed that we could find an equivalent gap for having the same decreased coupled effects (Figure 25). Therefore, we used a gap $G = 1\text{mm}$ length since the S_{21} in inline topology with 1mm gap is almost the same for the perpendicular one with $G = 0.1\text{mm}$ length (Figure 21).

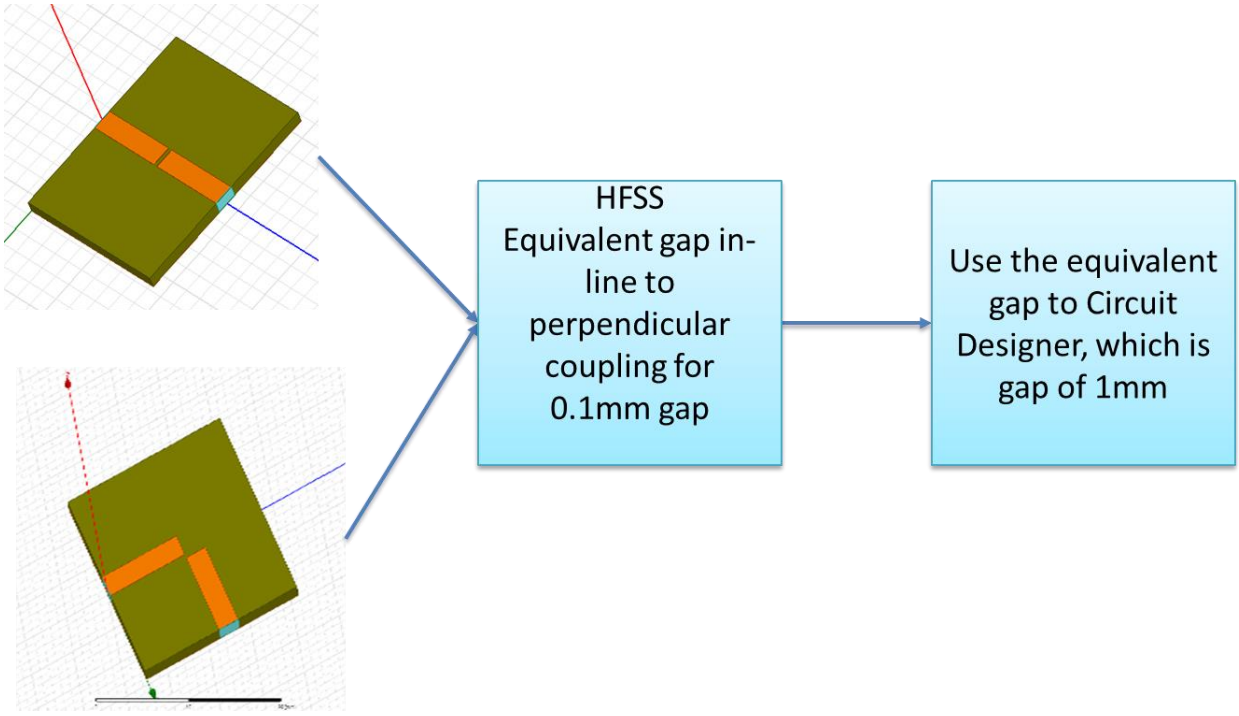

Figure 25: Using the equivalent length of gap in the in-line topology to achieve the same insertion loss for a perpendicular topology with gap=0.1mm

After this assumption, we simulated again a transient analysis, although this time we changed the gap from 0.1mm to 1mm (Figure 26).

As was observed on HFSS, a perpendicular alignment of the input and output microstrip lines with a gap of $G_p = 0.1\text{mm}$ is equivalent to a gap between linearly-aligned input and output microstrip lines of $G_l = 1mm$. In order to analyze the full circuit (with the diode), we now need to use Designer. Circuit Designer provides a model for the diode, but not one for the perpendicularly aligned input-output microstrip lines. In this case, then, we will simulate the circuit using in-line microstrip lines with the GAP element defining the coupling. For the separation between the gaps, we will use a "linear" distance equivalent to a perpendicular gap $G_p = 0.1mm$. As stated in the previous section, this is a gap $G_p = 0.1\text{mm}$. In both cases, the insertion loss is $S_{11} = -34\text{dB}$.

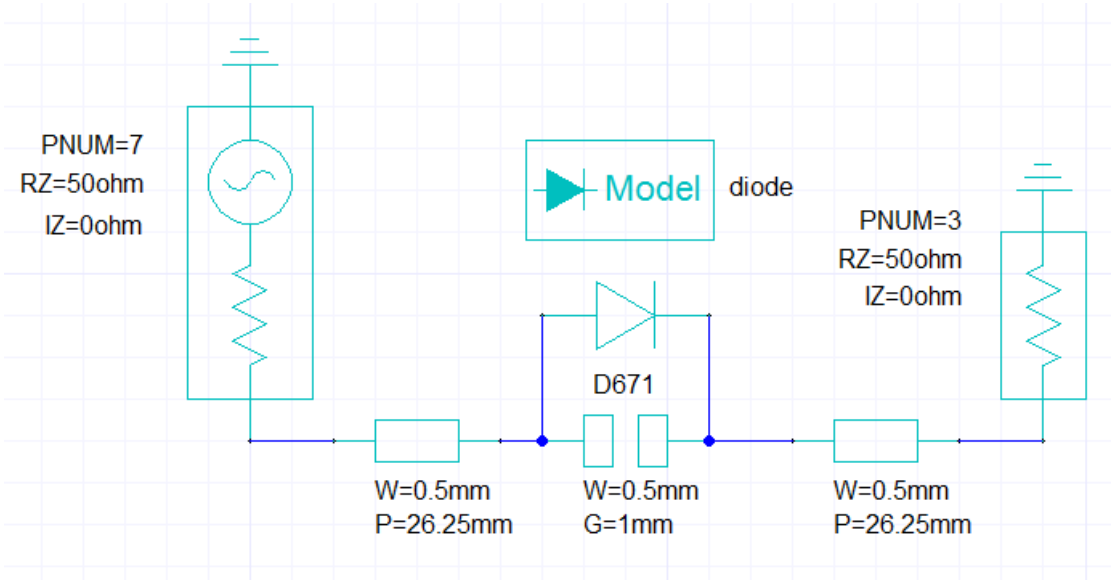

Figure 26: Two microstrip lines with width=0.5mm, length=26.25mm each and gap between them 1mm.

The results now show that the coupling has been minimized since there is no negative output signal (Figure 27).

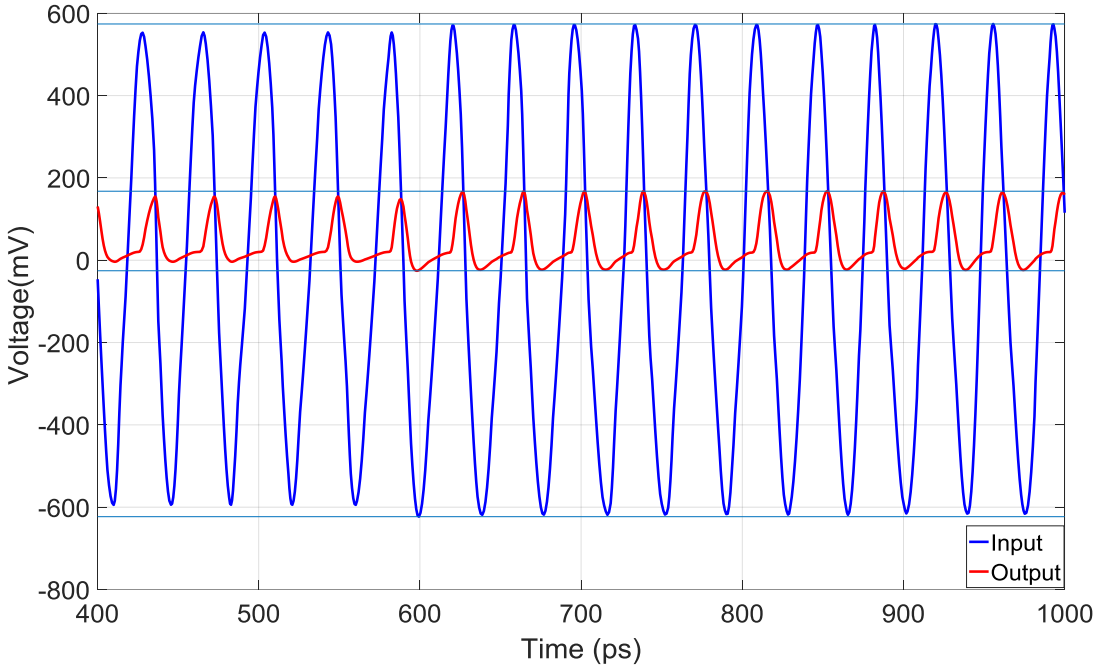

Figure 27: Transient analysis with input 900mV and gap 1mm on circuit Designer

Section 7.1: Circuit Analysis

We then run a circuit analysis inserting ideal lumped components to the design (Figure 28). Using the same dimensions for the microstrip lines, we added a resistor $R_L = 100\ ohm$ as the internal resistor of the rechargeable battery. Moreover, a capacitor $C_{sm} = 10\ pF$ is added to smooth the output signal to a DC one. For the output DC voltage, we have $V_{out} = 90.53\ mV$ (Figure 29), while the current is $I_{out} = 0.9mA$ (Figure 30).

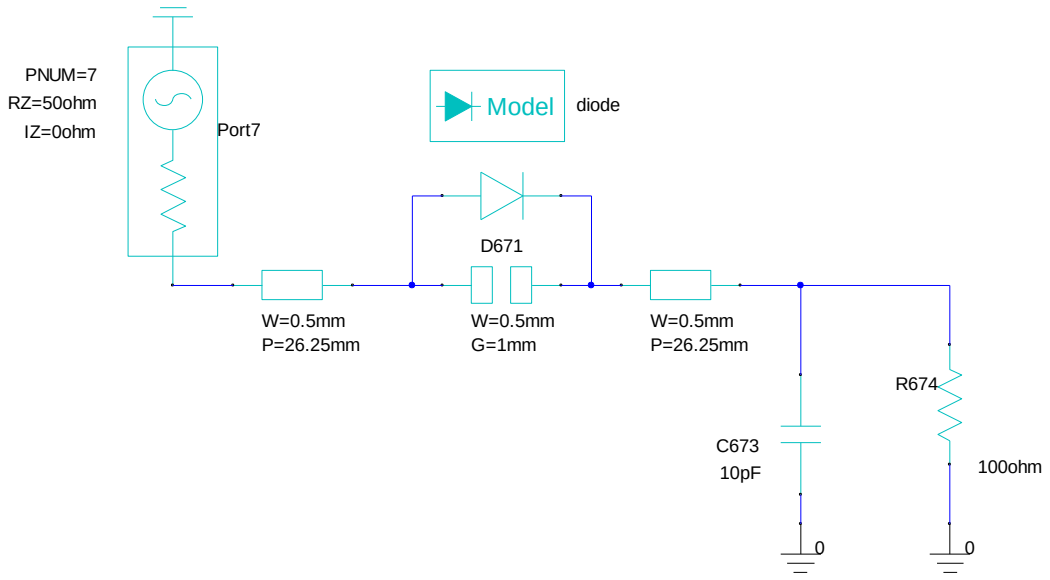

Figure 28: A rectifier circuit with microstrip lines and lumped ideal components

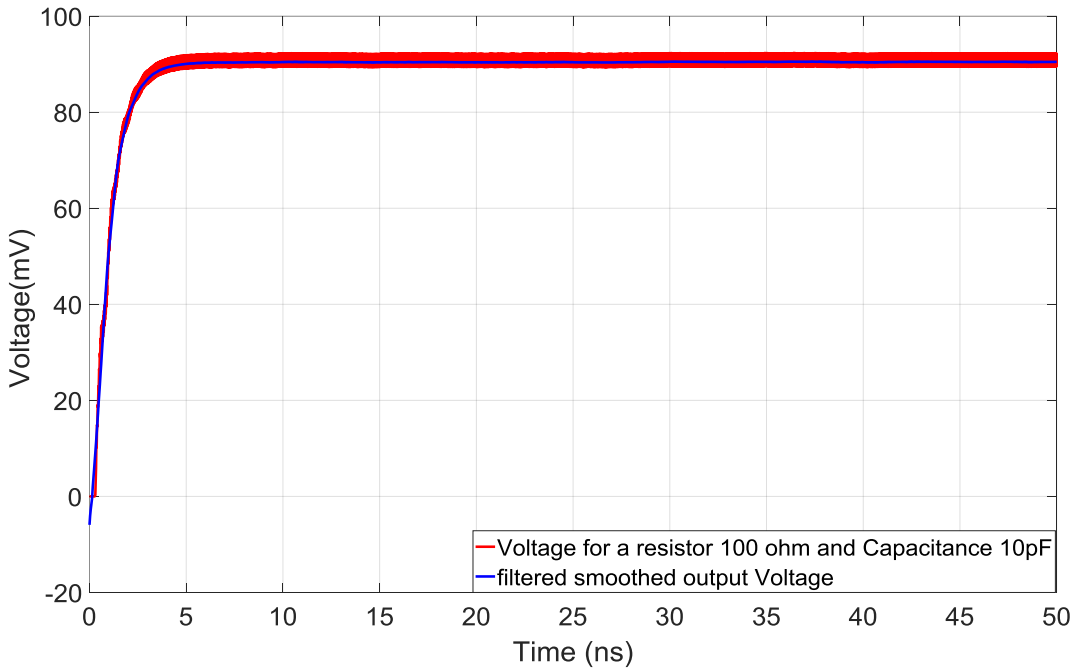

Figure 29: Voltage for a resistor 100 ohm and Capacitance 10pF

Then we have the same analysis for the current as we can see on the figure (Figure 30):

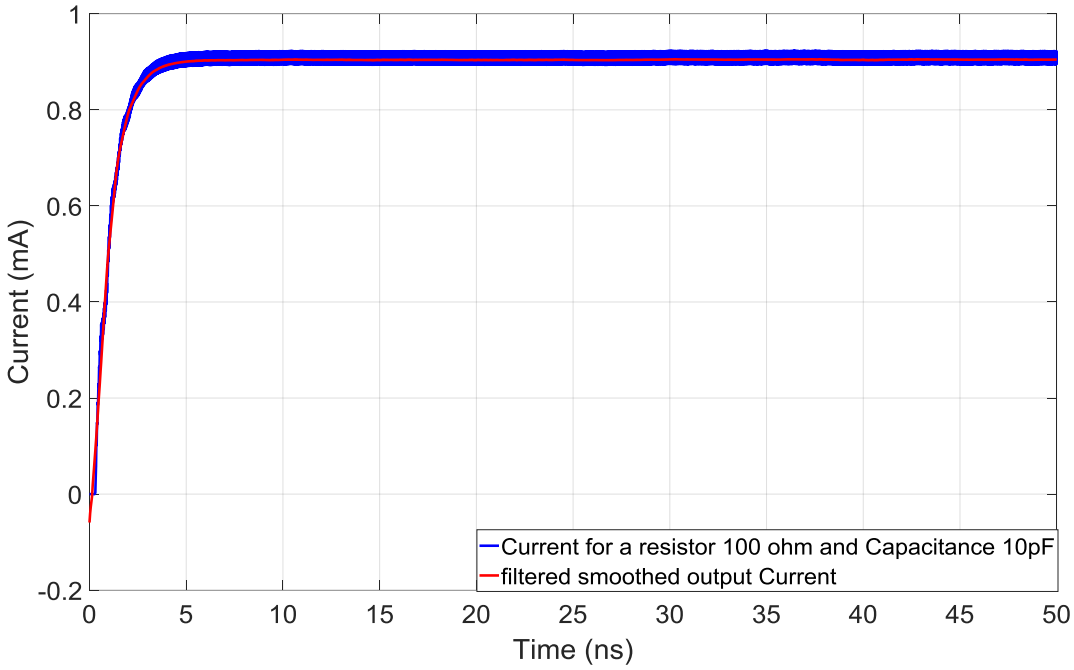

Figure 30: Current for a resistor 100 ohm and Capacitance 10pF

The voltage ripple for the circuit in Figure 24 is shown below:

$$V_r = \frac{V_p}{f * C * R} = \frac{247mV}{27.5\ GHz * 10pF * 100\ Ohm} = 8.9mV$$

Moreover, for the rectifier we need to show the RF-DC conversion efficiency.

$P_{DC} = \frac{{V_D}^2}{R_L} = \frac{90.53^2}{100} = 81.95\mu W$ RF-DC conversion

$\eta = \frac{P_{dc}}{P_{in}} = \frac{81.95\mu W}{1.492mW} = 5.4\%$ Efficiency

Chapter 8: Low Pass Filter after Diode

From Richard's transformation (Figure 31), we can see that one capacitor can be equivalent with one open stub following the equation below.

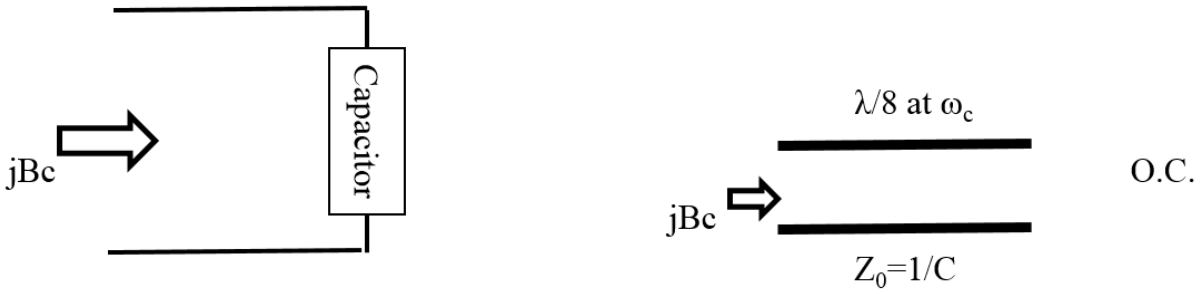

Figure 31: Richard's transformation for capacitor

$$Z_0 = \frac{1}{C * \omega_c}$$

Where:

Z_0 $is\ the\ impedance\ of\ the\ open\ stub\ in\ Ohm$

$C\ is\ the\ capacitance\ in\ pFarad$

$\omega_c\ is\ the\ angular\ frequency\ in\ the\ medium\ design\ in\ rad\ per\ second$

For our design, we need one open stub with length $\frac{\lambda_c}{8} = \frac{c}{8*f*\sqrt{e_r}} = 0.65mm$

Therefore, we design an open stub with length $P = 0.65mm$ and width $W = 1mm$ (Figure 32).

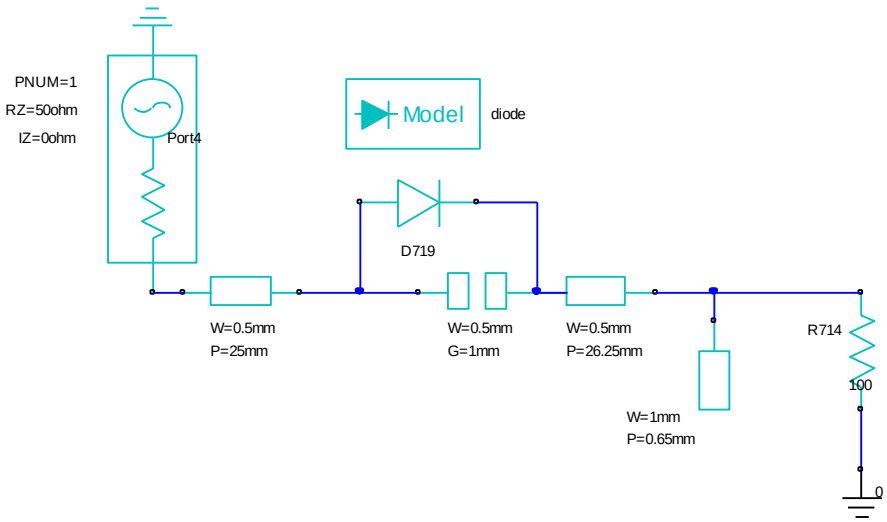

Figure 32: Proposed topology for distributed capacitor with one stub with 1mm width and 0.65mm length

We ran a transient analysis and graphed the output voltage for two stub widths: 1mm and 5mm widths. The fluctuations in the output signal were averaged, providing a value of 85.14mV for the 1mm width capacitor (Figure 33) and 82.19mV for the 5mm width capacitor (Figure 34). Fluctuations around the first average (1mm) were 140mV and the second (5mm) are 85mV. This shows that increasing the width of the capacitor provides better peak detection. However, the stub width would have to be increased to unrealistic levels to minimize fluctuations to reasonable levels. Instead, we increase the number of stubs, connecting them with transmission lines with the same width as the main microstrip line and length equal to the length of the stub (Figure 35).

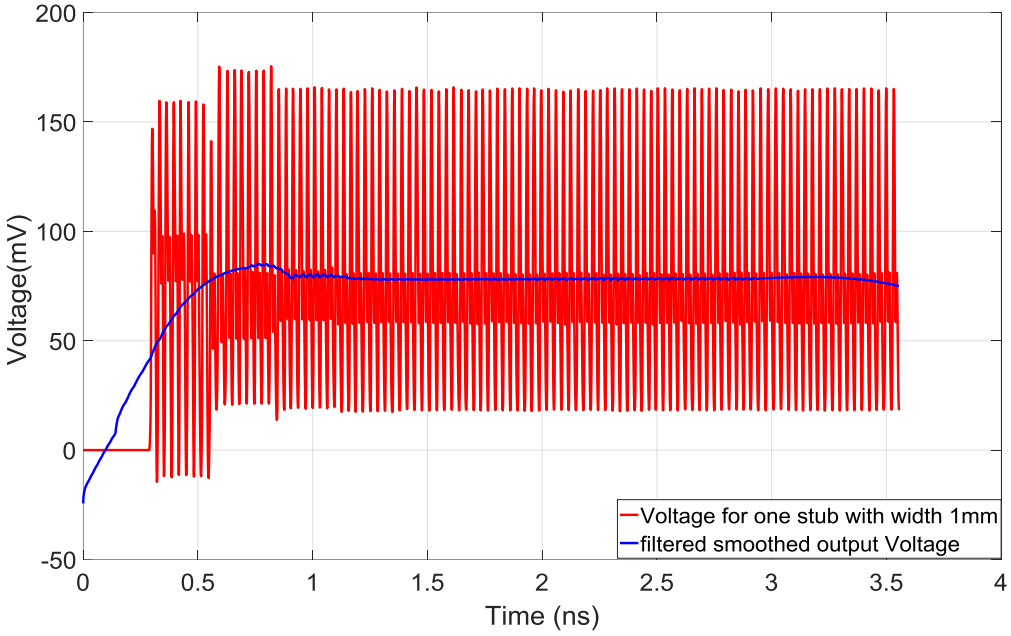

Figure 33: Voltage output for one stub with width 1mm, one Stub width 1mm yields fluctuation levels equal to 173% of smoothed value.

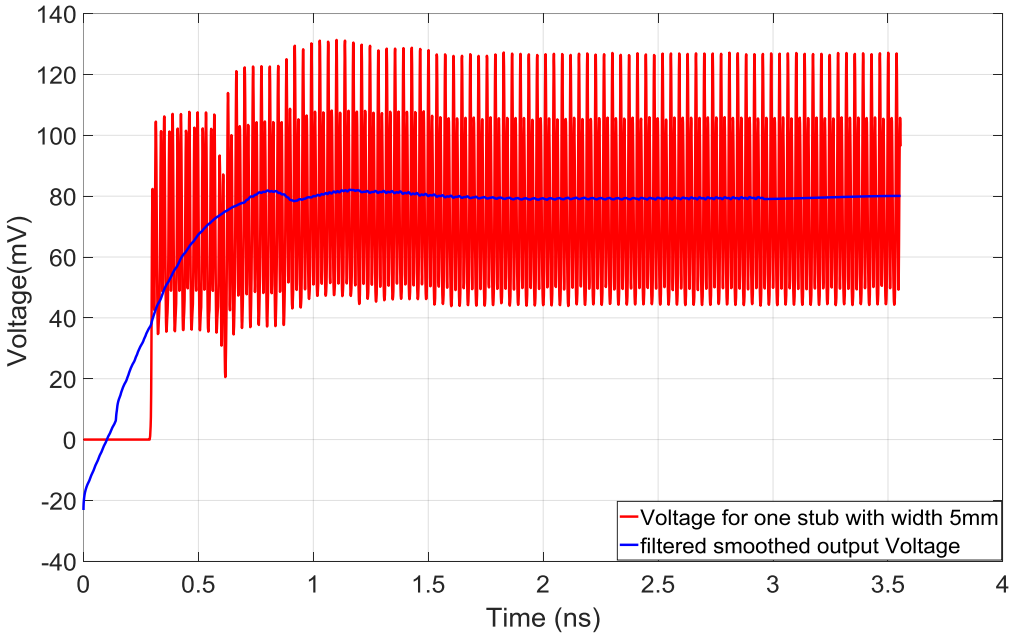

Figure 34: Voltage output for one stub with width 5 mm, one stub width 5mm yields fluctuation levels equal to 102% of smoothed output voltage.

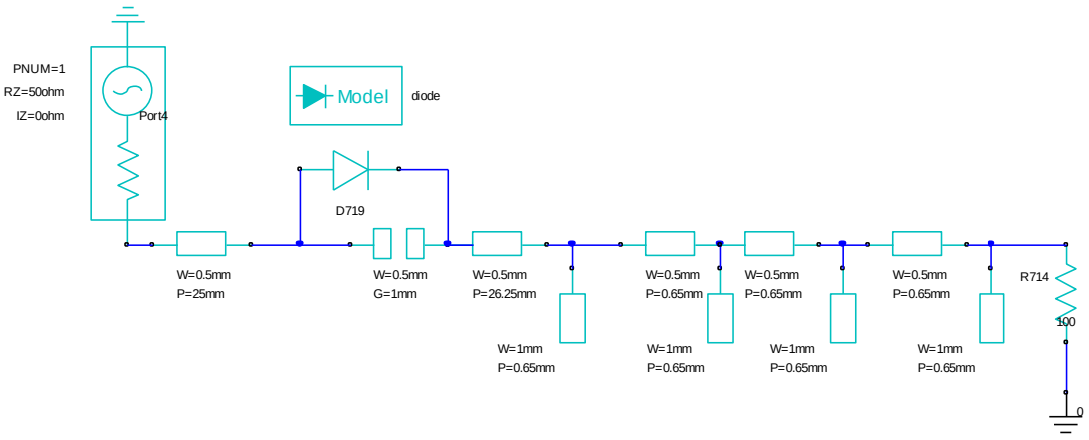

Figure 35: Proposed topology for distributed capacitor with four stubs with 1mm width and 0.65mm length

The maximum value of the smoothed-filter signal is 71.10mV for 1mm width (Figure 36) and 80mV for 5mm width (Figure 37). The range for the first one is 155mV and the second is 20mV the range. This shows that for four open stubs with width of 5mm the output voltage tends to be more DC.

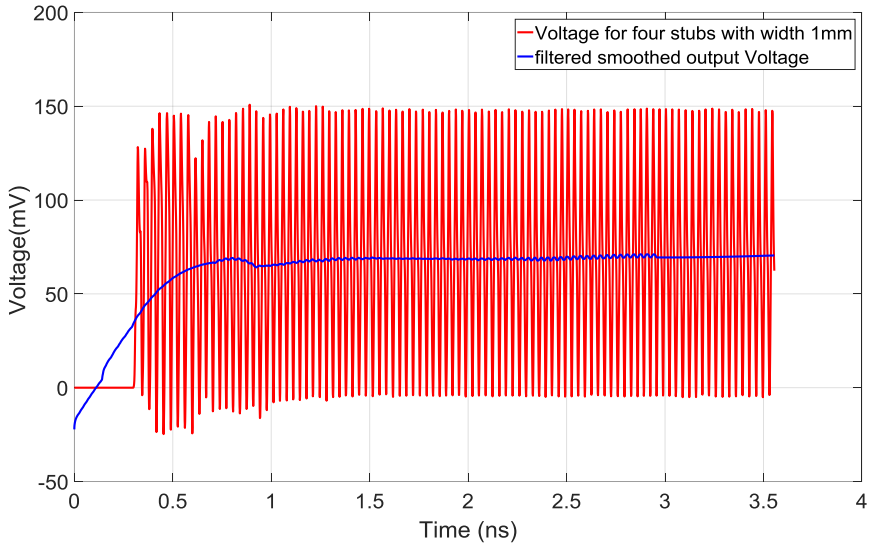

Figure 36: Voltage output for four stubs with width 1mm

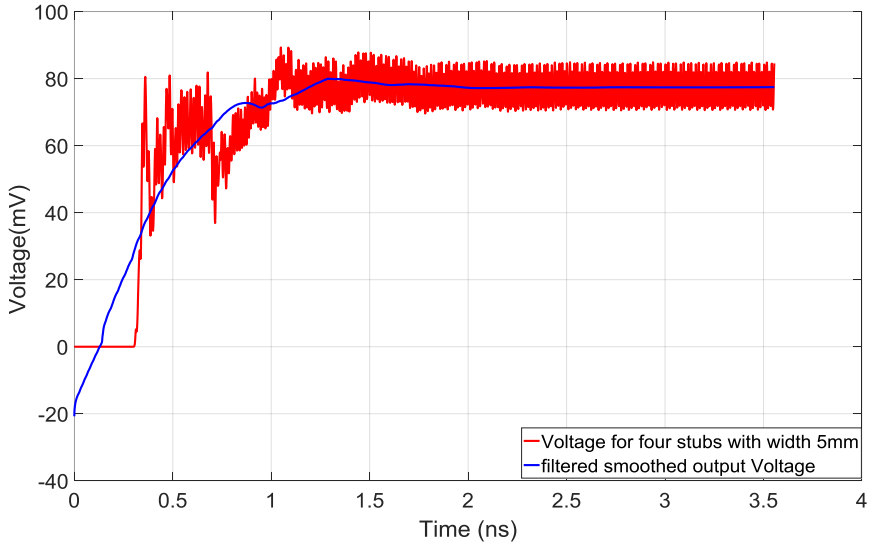

Figure 37: Voltage output for four stubs with width 5 mm 25% fluctuation

Chapter 9: Conclusion Future Work

To summarize, we designed and fabricated a rectenna operating in 5G where we used perpendicular input and output microstrip lines to minimize coupling, thus minimizing the size of the rectenna circuit. We also investigated the challenges that the design of circuits have in mmwave frequencies. Future work should focus on further refining the design of the antenna to allow for more effective signal harvesting, as well as investigating the design using a “real” source as opposed to an ideal, 27.5 GHz source.

References

[1] "Cellular frequencies in the US," [Online]. Available: https://en.wikipedia.org/wiki/Cellular_frequencies_in_the_US.

[2] 4. Americas, "5G Spectrum Recommendations," August 2015.

[3] R. E. Hattachi and J. Erfanian, "A Deliverable by the NGMN Alliance NGMN 5G white paper," 17-February-2015.

[4] Q. C. Li, H. Niu and A. T. Papathanassiou, "5G Network Capacity Key Elements and Technologies," in *IEEE Vehicular Technology Magazine*, 31 January 2014.

[5] e. w. paper, "5G systems, enabling the transformation of industry and society," January 2017.

[6] D. A. Osseiran, "The 5G Mobile and Wireless Commynication system," November 2013.

[7] H. W. Paper, "5G Opening up New Business Opportunities," August 2016.

[8] J. Zhang, X. Ge, Q. Li, M. Guizani and Y. Zhang, "5G Millimeter-Wave Antenna Array: Design and Challenges," in *IEEE Wireless Communications*, 20 October 2016.

[9] t. point, "5G 5th generation technology".

[10] "Wireless Power Transfer," [Online]. Available: https://en.wikipedia.org/wiki/Wireless_power_transfer.

[11] "Rectenna," [Online]. Available: https://en.wikipedia.org/wiki/Rectenna.

[12] J. Zhang and Y. Huang, "Rectennas for Wireless Energy Harvesting".

[13] C. Liu, Y.-X. Guo, H. Sun and S. Xiao, "Design and Safety Considerations of an Implantable Rectenna for Far-Field Wireless Power Transfer," in *IEEE Transactions on Antennas and Propagation*, 26 August 2014 .

[14] T. Campi, S. Cruciani, V. D. Santis and M. Feliziani, "EMF Safety and Thermal Aspects in a Pacemaker Equipped With a Wireless Power Transfer System Working at Low Frequency," *IEEE Transactions on Microwave Theory and Techniques*, 19 January 2016 .

[15] SEIKO, "Micro Battery Product Catalogue," 2017.

[16] "Computational electromagnetics," [Online]. Available: https://en.wikipedia.org/wiki/Computational_electromagnetics.

[17] W. Gibson, in *The Method of Moments in Electromagnetics*, Taylor & Francis Group, LLC.

[18] *Ansys ® Electronics Desktop 2016.2.0.*

[19] A. Bondeson, T. Rylander and P. Ingelstrom, "The Finite Element Method," in *Computational electromagnetics*, Springer.

[20] N. F. M. Aun, P. J. Soh, A. A. Al-Hadi, M. F. Jamlos, G. A. Vandenbosch and D. Schreurs, "Revolutionizing Wearables for 5G: 5G Technologies: Recent Developments and Future Perspectives for Wearable Devices and Antennas," in *IEEE Microwave Magazine*, 5 April 2017.

[21] D. Muirhead, M. A. Imran and K. Arshad, "A Survey of the Challenges, Opportunities and Use of Multiple Antennas in Current and Future 5G Small Cell Base Stations," in *IEEE Access* , May 17, 2016,.

[22] C. A. Balanis, Antenna Theory Analysis and Design, Wiley-Interscience, 2005.

[23] Macom, "MA4Exxxx Series," [Online]. Available: https://cdn.macom.com/datasheets/MA4Exxxx%20Series.pdf.

[24] A. Mavaddat, S. H. M. Armaki and A. R. Erfanian, "Millimeter-Wave Energy Harvesting Using 4*4 Microstrip Patch Antenna Array," *IEEE Antennas and Wireless Propagation Letters,* 12 November 2014 .

[25] H. Mei, X. Yang, B. Han and G. Tan, "High-efficiency microstrip rectenna for microwave power transmission at Ka band with low cost," in *IET Microwaves, Antennas & Propagation* , 15 December 2016.

[26] S. Ladan, A. B. Guntupall and a. KeWu, "A High-Efficiency 24 GHz Rectenna Development Towards Millimeter-Wave Energy Harvesting and Wireless Power Transmission," in *IEEE transactions on circuits and systems*, 2014.

[27] S. Ladan, S. Hemour and K. Wu, "Towards Millimeter-Wave High-Efficiency Rectification for Wireless Energy Harvesting," in *Wireless Symposium (IWS), 2013 IEEE International*, 2013.